Available online at www.sciencedirect.com
SCIENCE DIRECT
Polymer 46 (2005) 9304–9313
polymer
www.elsevier.com/locate/polymer

Synthesis of rod-coil diblock copolymers by ATRP and their honeycomb morphologies formed by the 'breath figures' method

Chen-Lung Lin, Pao-Hsiang Tung, Feng-Chih Chang*

Institute of Applied Chemistry, National Chiao Tung University, Hsinchu, Taiwan, ROC

Received 20 March 2005; received in revised form 13 July 2005; accepted 14 July 2005
Available online 8 August 2005

Abstract

We have synthesized rod-coil diblock PPQ-*b*-PMMA copolymers by using the versatile atom-transfer radical polymerization method and have characterized them by differential scanning calorimetry (DSC), Fourier transform infrared spectroscopy (FTIR), and thermogravimetric analysis (TGA). The methyl ketone-terminated rod-coil diblock PMMA copolymer has a higher value of T_g, because of its syndiotactic-like structure, and a higher decomposition temperature than does the PMMA homopolymer. The presence of the PPQ block tends to retard the early decomposition of the PMMA chain. A regularly porous, honeycomb-structured film was prepared from the dichloromethane solution of the diblock copolymers under a flow of moist air. The diameters of the spherical pores can be controlled in the range from 0.8 to 3 μm by modifying both the rod-coil copolymers' relative molecular weights and the casting conditions. The wall thickness of the film is varied linearly with the relative molecular mass (M_r).

Keywords: ATRP; PPQ-*b*-PMMA copolymers; Honeycomb-structured film

1. Introduction

During the last few decades, block copolymers have attracted an increasing amount of interest both from scientific and commercial points of view [1,2] because of their highly symmetrical morphological behavior on length scales ranging between a few nanometers and several hundreds of nanometers. In recent years, the rod-coil diblock copolymers have been developed that exhibit unique morphologies and phase separation behavior [3–7]. The difference in the chain rigidity of the rod-like and coil-like blocks greatly affects aspects of the molecular packing and the thermodynamically stable morphologies of these materials. Apart from the wide range of different self-assembling structures that form, another unique characteristic of these materials is that the rod segments can endow various functionalities, such as photophysical and electrochemical properties, to the materials. Incorporation of π-conjugated polymer chains into heterogeneous diblock copolymers can create new materials that present promising nonlinear optical, photoconductive, and electroluminescence properties [8–10].

Porous materials with a perfect arrangement of pores provide interesting properties for various technological applications such as photonic bandgap materials, heterojunction devices, and picoliter beakers. Picoliter beakers [11–14] are of importance in analytical and bioanalytical chemistry because they allow isolating very small volumes of liquid or single cells and interrogating them by either electrochemical or enzymatic methods. However, the fabrication of ordered mesoporous/microporous solids is not trivial and often involves tedious photolithographic methods or templating using emulsions [15] that are expensive and complicated. On the contrary, microporous structures can be fabricated by a simple self-organization technique using star polymers [16], amphiphilic copolymers [17], or rod-coil block copolymers [18] in a moist atmosphere. As mentioned above, the rod-coil block copolymer has more advantage to form porous materials because the rod segment can be cross-linking to render them insoluble [19] or endow conductive property [20].

* Corresponding author. Tel.: +886 3 572 7077; fax: +886 3 571 9507.
E-mail address: changfc@mail.nctu.edu.tw (F.-C. Chang).

0032-3861/$ - see front matter © 2005 Elsevier Ltd. All rights reserved.
doi:10.1016/j.polymer.2005.07.051

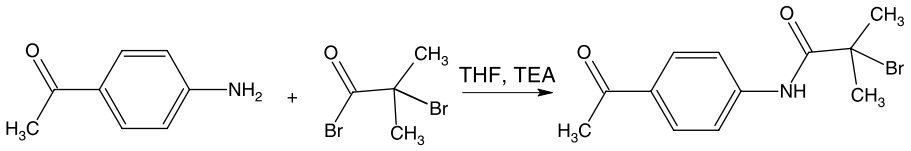

(1)

Scheme 1.

The preparation of rod-coil block copolymers consisting of conjugated rods is a great challenge in polymer synthesis because it is difficult to connect these two physically and chemically different blocks. Traditionally, polymer chains possessing terminal functional groups are prepared by controlled termination of living ionic polymerizations but because of the extreme sensitivity that living ionic polymerization displays to impurities and functional groups, strict experiments are necessary. Atom-transfer radical polymerization (ATRP) is an efficient technique for polymerizing various monomers in a controlled manner to yield polymers that have predetermined molecular weights and narrow polydispersity [21]. Since, various ATRP initiators can be modified to fulfill the requirements of the linking bridge molecules of rod-coil copolymers, we chose to synthesize a flexible methyl ketone-terminated polymer chain and then to connect it to poly(phenylquinoline) (PPQ).

In this study, we first synthesized a methyl ketone-terminated poly(methyl methacrylate) (PMMA) and then used its ketone groups as linkage units with which to connect PPQ chains through a condensation reaction. The polymers were characterized by gel permeation chromatography (GPC), Fourier transform infrared spectroscopy (FTIR), thermogravimetric analysis (TGA), and differential scanning calorimetry (DSC) measurements. When the polymer was then cast into thin film using appropriate solvents on solid substrates, highly ordered, micro-porous honeycomb structures formed spontaneously; the empty spherical cells had diameters ranging from 0.8 to 2.5 μm.

2. Experimental section

2.1. Materials

MMA (SHOWA, 99%) was passed through a basic activated alumina column and distilled from CaH_2 before use. Copper (I) bromide was purified according to a literature procedure [22]. *N*,*N*,*N*′,*N*″,*N*‴-Pentamethyldiethylenetriamine (PMDETA, TCI, 98%), xylene (MEDIA, 99%), 1-(4-aminophenyl)ethanone (ACROS, 99%), and 2-bromo-2-methylpropanoyl bromide (TCI, 99%) were all commercial products and were used without further purification. 5-Acetyl-2-aminobenzophenone (**2**) was synthesized according to a literature procedure [23].

2.2. Synthesis of N-(4-acetylphenyl)-2-bromo-2-methylpropanamide (*1*)

A dry 100 mL round-bottom flask equipped with a stirrer bar was charged with dry THF (40 mL), 1-(4-aminophenyl) ethanone (6.76 g, 50 mmol), and dry triethylamine (6.75 mL, 50 mmol). The solution was cooled to 0 °C in an ice bath and then 2-bromo-2-methylpropanoyl bromide (13.8 mL, 60 mmol) in dry THF (30 mL) was added dropwisely using a dropping funnel (Scheme 1) to form a white precipitate. The slurry was stirred at room temperature for 3 h before being filtered. The solvent was evaporated under reduced pressure to yield a brown precipitate, which was then dissolved in EtOAc and washed three times with water. After one recrystallization from

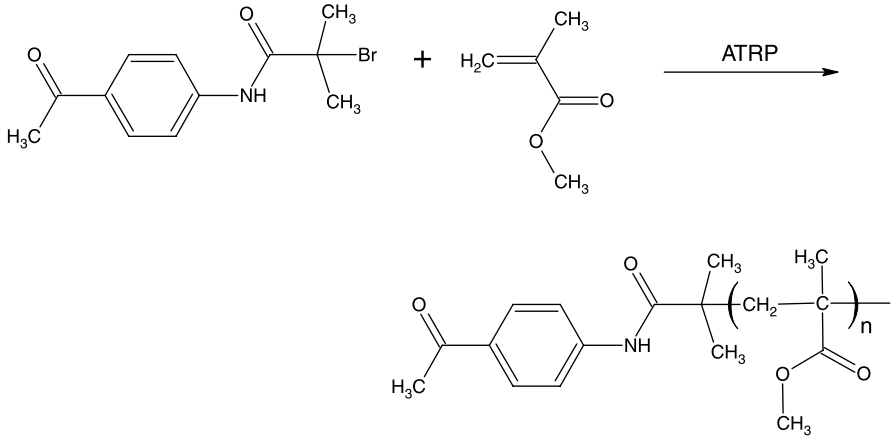

Scheme 2.

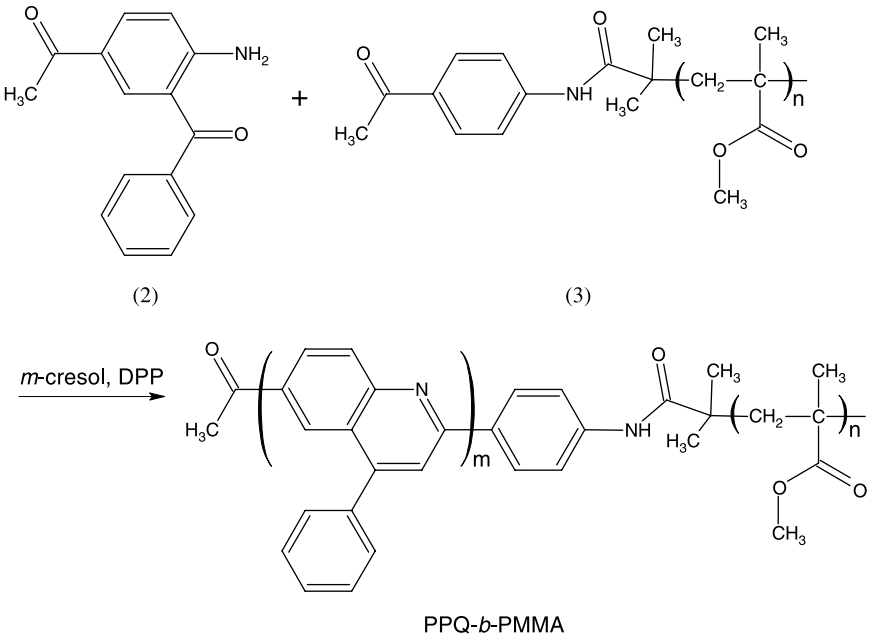

Scheme 3.

EtOAc/hexane, pure (**1**) was obtained (12.2 g, 86%): Mp 129.4–132.3 °C; FTIR (KBr, pellet) 3322 (N–H), 1676 (C=O) cm^{-1}; ^1H NMR (500 MHz, $CDCl_3$) δ 8.6 (br, 1H, N*H*), 7.9 (d, 2H, aryl), 7.6 (d, 2H, aryl), 2.6 (s, 3H, $COCH_3$), 2.0 [s, 6H, $CBr(CH_3)_2$].

2.3. Polymerization of methyl ketone-terminated poly(-methyl methacrylate) (*3*)

We prepared a polymerization system having $[M]_0$:$[I]_0$ of 800:1 by charging MMA (10.75 mL, 100 mmol), CuBr (17.7 mg, 0.125 mmol), *N*-(4-acetylphenyl)-2-bromo-2-methylpropanamide (**1**; 35.5 mg, 0.125 mmol), and xylene (2.5 mL) into a reaction flask equipped with a magnetic stirrer bar (Scheme 2). The flask was sealed with a rubber septum and degassed by three freeze-pump-thaw cycles. The reaction flask was immersed in an oil bath at 80 °C and then PMDETA (52 μL, 0.25 mmol) was added by syringe. As the viscosity increased, the stirrer bar eventually stopped rotating, but the reaction continued and we collected the last sample after 12 h. After cooling to room temperature, THF was added to the reaction mixture to dissolve the polymer. The product was precipitated by pouring the solution into a large excess of methanol.

2.4. Synthesis of poly(phenylquinoline)-block-poly(methyl methacrylate) diblock copolymer

PPQ-*b*-PMMA diblock copolymers were synthesized by copolymerization of 5-acetyl-2-aminobenzophenone (**2**) with (**3**) as presented in Scheme 3. A round-bottom flask was charged with (**2**) (0.12 g, 0.5 mmol), (**3**) (3.25 g, 0.025 mmol), diphenyl phosphate (DPP, 0.3 g), and freshly distilled *m*-cresol (4 mL). The temperature of the mixture was raised slowly to 140 °C over 3 h. Additional DPP was added as the viscosity of the mixture increased with time; a total of 1.25 g of DPP was added. The reaction mixture's temperature was maintained at 140 °C for 72 h under argon atmosphere. In general, the condensation reaction yield of copolymerization is 100% [18]. The product was precipitated by pouring the mixture into 10% triethylamine/ethanol (100 mL) and then purified by the Soxhlet extraction with 10% triethylamine/ethanol for 48 h and THF for additional 72 h. The final diblock copolymer was collected from the THF-soluble product.

2.5. Measurements

Molecular weights and molecular weight distributions were determined by GPC using a Waters 510 HPLC equipped with a 410 differential refractometer, a UV detector, and three ultrastyragel columns (100, 500, and 10^3 Å) connected in series and using THF as the eluent at a flow rate of 0.4 mL/min. The molecular weight calibration curve was obtained using polystyrene standards. ^1H NMR spectroscopy was performed using an INOVA 500 instrument; $CDCl_3$ was the solvent. Infrared spectra were obtained using a Nicolet Avatar 320 FT-IR spectrometer. A differential scanning calorimeter (Du-Pont TA 2010 instrument) was used to determine the thermal transitions at a heating rate of 20 °C/min^{-1}. The TGA thermograms were obtained on a Du-Pont TA Q-50 instrument at a heating rate of °C/min^{-1} under nitrogen. Polarized optical transmission microscopy was performed on an Olympus BX50 microscope equipped with digital camera (Olympus PD12). Prior to imaging by SEM, the samples were coated

Table 1
Molecular weights and thermal properties of the methyl ketone-terminated PMMA

	Time (h)	Conv. (%)	$M_{n,\ GPC}$	$M_{n,\ NMR}$	M_w/M_n	T_g
$PMMA_{800}$	12	85	78,600	80,100	1.28	129
$PMMA_{1300}$	12	74	127,000	128,000	1.34	127
$PMMA_{2500}$	16	60	230,800	246,500	1.35	128

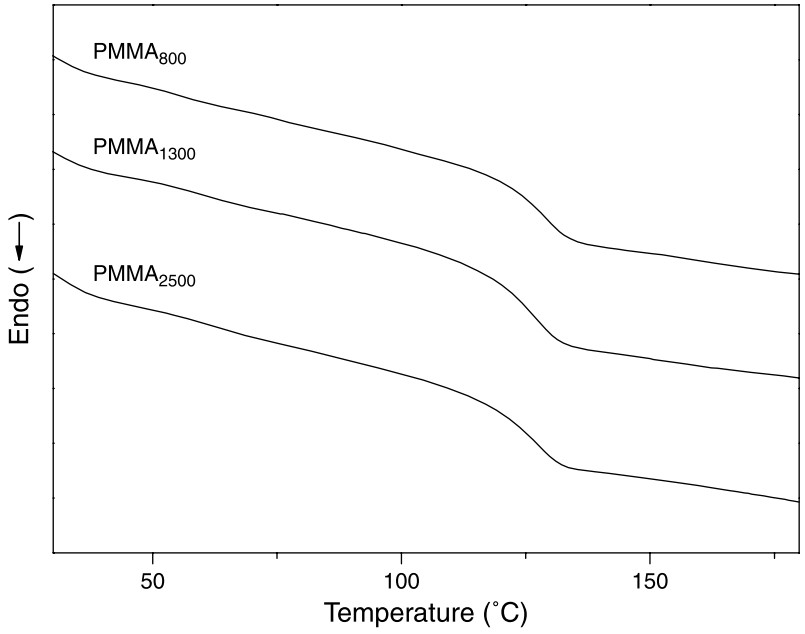

Fig. 1. DSC scans of PMMAs having various degrees of polymerization.

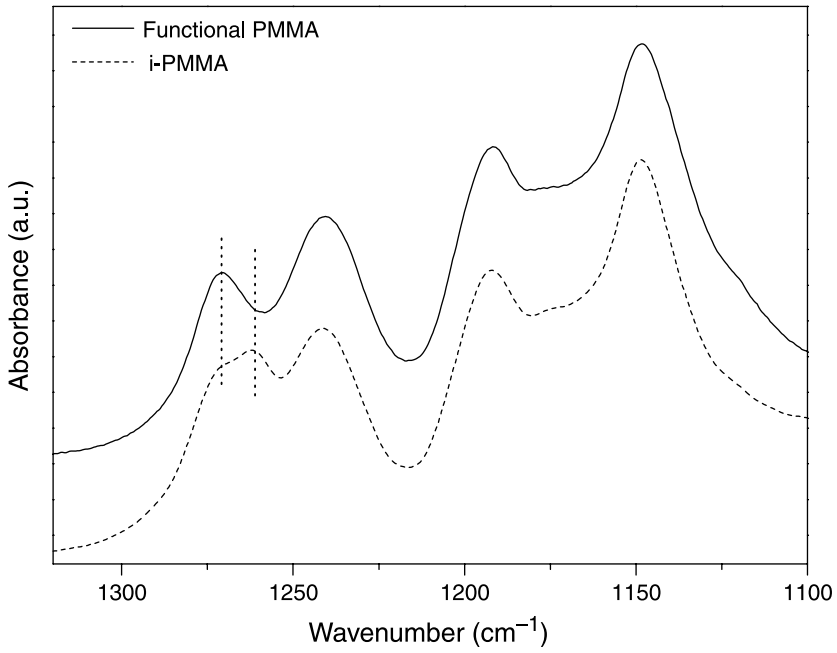

Fig. 2. Infrared absorbances of PMMAs having different tacticities. The curve having the solid line represents the syndiotactic-like methyl ketone-terminated PMMA; the dashed line represents that of the isotactic-like PMMA (the isotactic-like PMMA was synthesized in our laboratory through the use of a different initiator for ATRP).

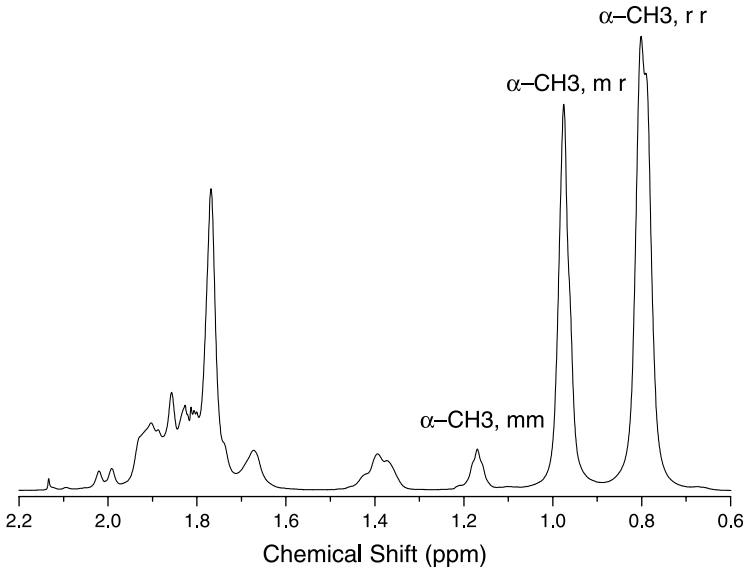

Fig. 3. ^{1}H NMR spectrum of the $PMMA_{1300}$.

with Pt (10 nm). SEM images were recorded using a TOSHIBA S4700I field emission microscope working at a voltage of 5 kV and a beam current of 1×10^{-10} A.

3. Results and discussion

3.1. Synthesis of methyl ketone-terminated PMMA and rod-coil diblock polymers

A functional PMMA derivative was polymerized by ATRP, which has been demonstrated to be an efficient method for performing living polymerizations of a large number of monomers. The polymerization, which is depicted in Scheme 2, was carried out by using CuBr, complexed by PMDETA, as the catalyst in xylene solution at 80 °C and was initiated by the action of *N*-(4-acetylphenyl)-2-bromo-2-methylpropanamide (**1**). The molecular weights and polydispersities of the functionalized PMMAs were characterized by GPC. We performed additional molecular weight measurements by ^{1}H NMR spectroscopy by analyzing the relative intensities of the signals of the protons of both the initiator and PMMA; in particular, we performed these calculations by comparing

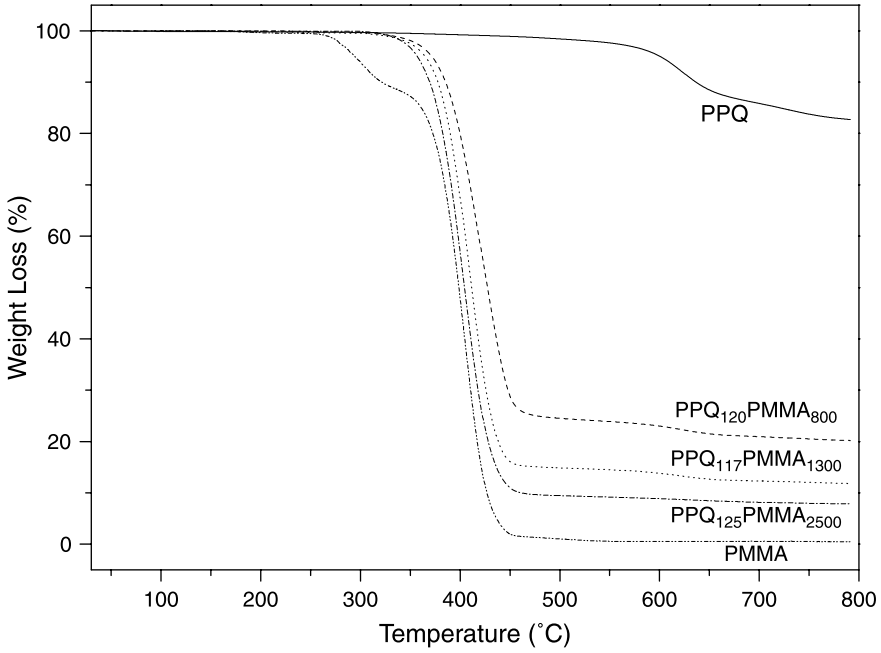

Fig. 4. TGA thermograms of PPQ, methyl ketone-terminated PMMA, and rod-coil diblock copolymers under a flow of N_2 at 20 °C/min.

Table 2
Yields of diblock copolymers calculated after solvent extraction

	Yield (%)	T_g (°C)	T_d (5% weight loss under N_2) (°C)	Residual weight at 500 °C (%)		M_r (PPQ/PMMA)
				Calculated	Measured	
$PPQ_{50}PMMA_{800}$	77	127	362.2	4.9	11.5	0.13
$PPQ_{120}PMMA_{800}$	79	130	367.9	13.3	23.8	0.31
$PPQ_{48}PMMA_{1300}$	72	130	364.6	3.1	6.8	0.07
$PPQ_{117}PMMA_{1300}$	74	128	360.7	8.6	14.9	0.18
$PPQ_{52}PMMA_{2500}$	76	129	351.6	2.1	4.1	0.04
$PPQ_{125}PMMA_{2500}$	77	128	352.1	6.9	9.5	0.1

The values of T_g and T_d and the residual weights were measured and calculated from DSC and TGA measurements. M_r, molecular ratio of PPQ blocks/PMMA blocks.

the signals between 7.4 and 8 ppm, due to the aromatic protons of the initiator, with those at 3.5 ppm for the methyl ester groups of the PMMA segments. The calculated values, which are presented in Table 1, provide results that agree well with those obtained by GPC. In this table, the subscript n of the descriptor '$PMMA_n$' reflects the degree of polymerization.

From Fig. 1, the T_g obtained by DSC for the functionalized PMMA is higher than that of commercial PMMA by ca. 20 °C. In general, the glass transition temperature of PMMA is proportional to the degree of syndiotacticity and inversely proportional to the degree of isotacticity. The higher ratio of syndiotacticity results in a relatively regular structure and leads to an increase in the glass transition temperature. The FTIR analysis were performed to interpret the reasons for the observed higher T_g. Absorptions in the range 1300–1100 cm^{-1} of the FTIR spectrum are sensitive to the tacticity of PMMA [24]; e.g. syndiotactic and isotactic PMMA present different absorption peaks, at 1270 and 1260 cm^{-1}, respectively. Because of its highly restricted backbone conformation, syndiotactic PMMA has a higher absorption frequency at 1270 cm^{-1} and larger value of T_g than does isotactic PMMA. Fig. 2 presents the FTIR spectra of PMMA with various tacticities; it reveals that the functional PMMA we synthesized has a characteristic peak at 1270 cm^{-1} and, hence, our functional PMMA is favoring a syndiotactic structure. ^1H NMR was also used to characterize the tacticities of PMMA. The methylene and α-methyl proton spectra of the functional $PMMA_{1300}$ were shown in Fig. 3. It displays three distinct peaks appearing at the highest field, which represent methacrylate methyl groups of different tacticity [25]. The bands at about 0.8, 0.98, and 1.17 ppm arise from syndiotactic (rr), atactic (mr), and isotactic (mm) methyl groups, respectively. From Fig. 3, the tacticity of the $PMMA_{1300}$ was calculated from the integrated ratios of rr, mr, and mm. The ratios of the triad tacticty for syndiotactic, atactic, and

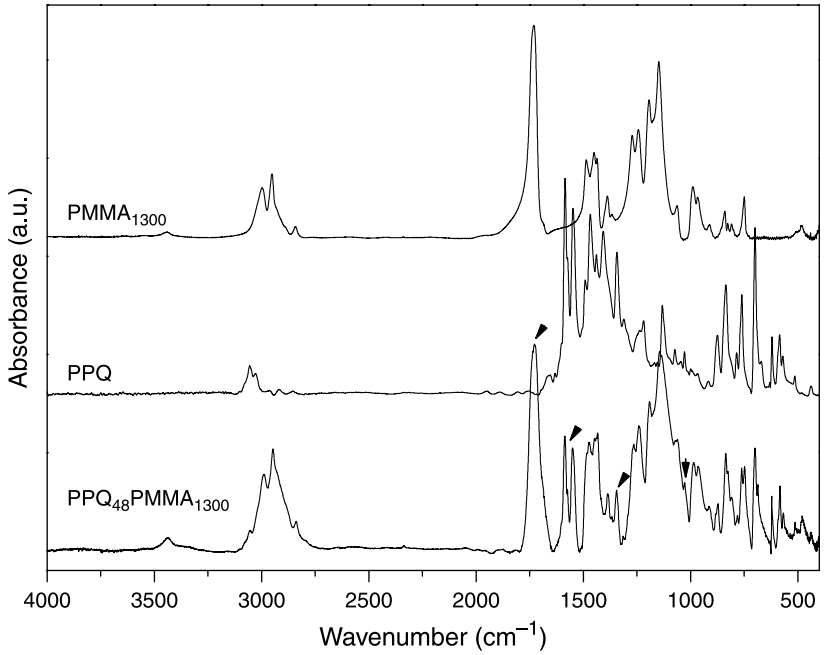

Fig. 5. FTIR spectra of methyl ketone-terminated PMMA, the PPQ homopolymer, and the rod-coil diblock copolymer. The arrows indicate the characteristic absorption peaks of the diblock copolymer.

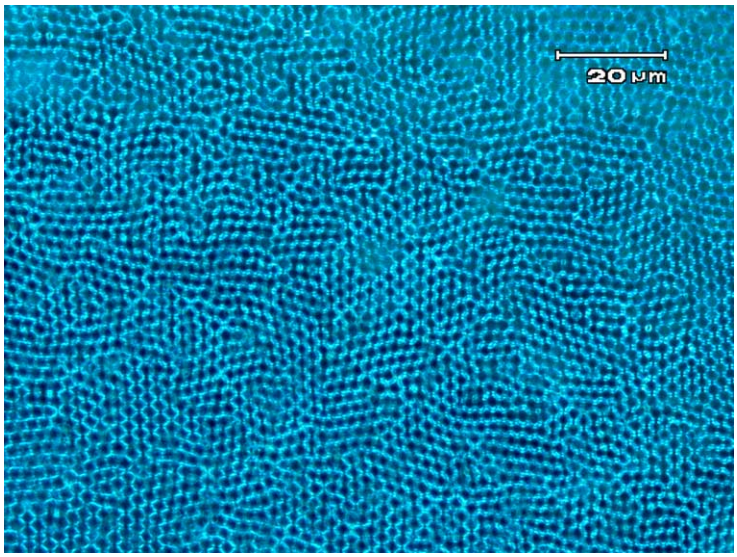

Fig. 6. POM images prepared by dichloromethane solution of $PPQ_{52}PMMA_{2500}$ at concentration of 0.5 wt% under humidity of 73%.

isotactic are 60.9, 35.5, and 3.6, respectively. According to these results, the functional PMMA has a syndiotactic-favoring configuration and possesses the higher value of T_g.

Scheme 3 outlines our synthetic approach to PPQ-*b*-PMMA. Although the polymerization of the PPQ block is a condensation-type reaction, the composition of the resultant diblock copolymer could be controlled by the stoichiometry. The reaction product was purified by Soxhlet extraction using a TEA/EtOAc solution; with this technique, we washed out PPQ-*b*-PMMA copolymers that had low degrees of polymerized PPQ blocks and any unreacted functionalized PMMAs. Furthermore, we separated the product into THF-soluble and -insoluble parts by the Soxhlet extraction procedure. The final diblock copolymer was collected from the THF-soluble part. These procedures ensure that the copolymer obtained is a rod-coil diblock copolymer and not just a physical blend. As a result, the product yield was slightly below 80% (72–79%) after extraction.

We employed TGA to obtain the correct composition of the diblock copolymers [5]. Fig. 4 displays TGA

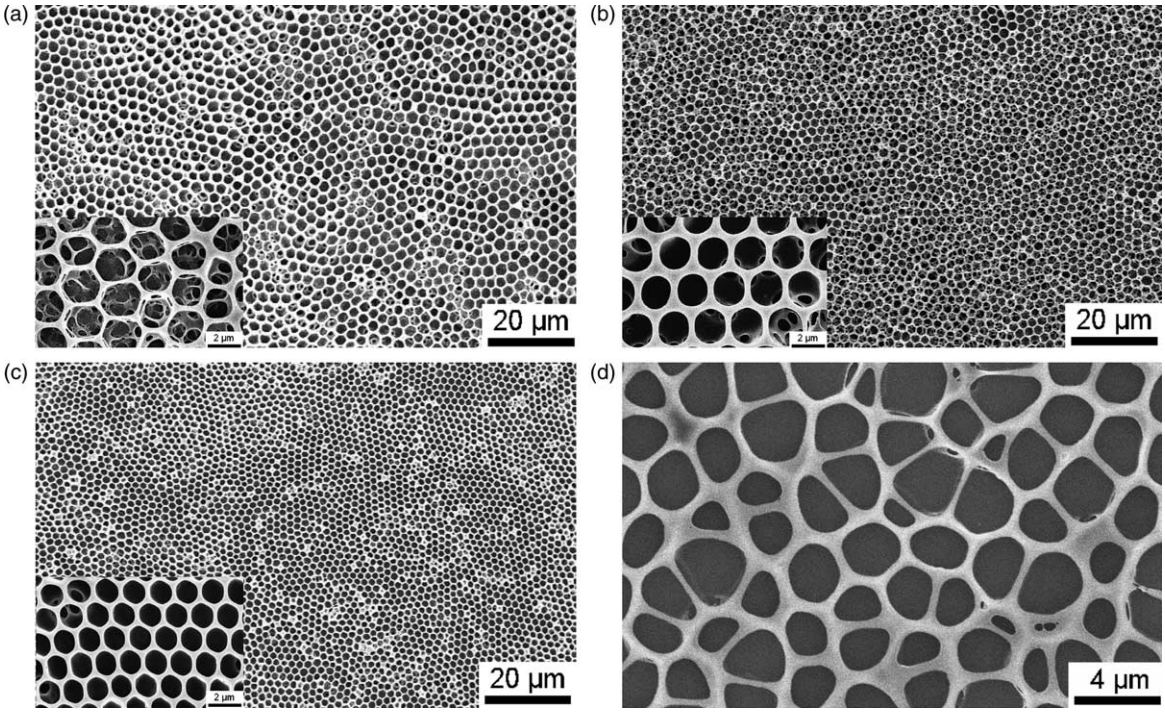

Fig. 7. SEM images prepared when using dichloromethane solutions of $PPQ_{52}PMMA_{2500}$ at different concentrations. (a) 0.1 wt%; (b) 0.5 wt%; (c) 1 wt%; (d) 0.005 wt%.

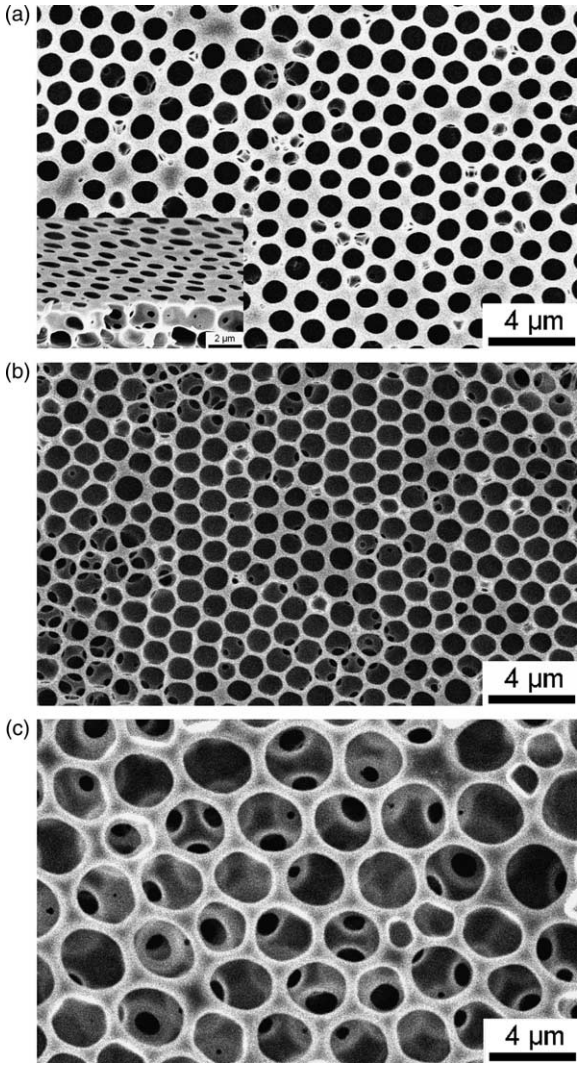

Fig. 8. SEM images prepared when using the same concentration (1 wt%) of different diblock copolymers. (a) $PPQ_{48}PMMA_{1300}$; (b) PPQ_{52}-$PMMA_{2500}$; (c) $PPQ_{50}PMMA_{800}$.

thermograms of these diblock copolymers; the corresponding thermograms of both the PPQ and PMMA homopolymers were also obtained for the sake of comparison. The 5%-weight-loss decomposition temperatures of PPQ and PMMA are 600 and 300 °C, respectively. The diblock copolymers undergo two-step decompositions under nitrogen. The first thermal decomposition temperature (300–450 °C) comes from the flexible PMMA block of the copolymer. After decomposition of this flexible block, the rigid PPQ block remains stable up to 600 °C, which is identical to the decomposition temperature of the PPQ homopolymer. Because the PMMA block is decomposed completely at 450 °C, the residual weight in the range from 450 to 550 °C is contributed by the PPQ block and, thus, the residual weight in this range can be used to calculate the composition of the diblock copolymer. Table 2 summarizes the calculated compositions (the subscripts n of 'PPQ_n' reflect the number of repeat units of the PPQ blocks). The improved thermal stability of the PMMA block in the diblock copolymers, relative to that of the parent PMMA homopolymer, can be understood as being a consequence of the tethering of the PMMA chain onto the rod chain. Hence, the PPQ, which possesses a higher decomposition temperature, can prevent the PMMA chain from degrading sooner. From the DSC measurement, we found that all of the diblock copolymers exhibit one glass transition, at 130 °C. We detected no crystalline melting or glass transition for the PPQ block before the decomposition temperature of the PMMA block was reached.

Fig. 5 indicates that the FTIR spectrum of the diblock copolymer is essentially a superposition of the spectra of the parent PMMA and PPQ homopolymers, but there are significant differences between the vibrational spectra of the methyl ketone-terminated PMMA and the PPQ homopolymer and, therefore, their contributions to the FTIR spectra of the diblock copolymers can be determined. The stretching bands at 1730 cm^{-1}, which we assign to the carbonyl group of the functionalized PMMA, appear in the FTIR spectrum of the diblock copolymer. The vibrational bands at 1585/1550 and 1345/1028 cm^{-1} are characteristic peaks of the phenyl and the quinoline rings of the PPQ block. Thus, the results obtained by FTIR, TGA, and DSC all confirm the structure of the rod-coil diblock copolymer.

3.2. Micro-porous honeycomb morphology

Usually when preparing micro-porous materials, colloidal crystals of polystyrene or silica spheres are used as templates that must be removed either by thermal decomposition or by solvent extraction [26–28]. Such an approach, however, is probably not useful for dynamically controlling virtual length scales. In this study, we used a simple and facile method, the so-called 'breath figure', to form ordered structures [29–37]. There are several factors may influence the formation of the honeycomb structure and different morphologies, including the concentration of the PPQ-PMMA solution, the relative humidity in the atmosphere, the rate of air flow, and the film formation temperature. In this study, effect of the PPQ-*b*-PMMA concentration and its relative molecular mass (M_r, the PPQ block relative to the PMMA block) were used to control the pore size of the resulted film.

Upon drop-casting a dichloromethane solution of the rod-coil diblock copolymer onto a glass slide in an air-flow hood, condensation of water on the cold surface of the liquid film was observed at relative humidities $>60\%$. After a few seconds, the whole surface of the solution began to scatter light, which turned the sample opaque. After complete evaporation of the solvent, the sample was characterized by polarized optical microscopy, as shown in Fig. 6, showing highly ordered, hexagonal, close-packed pores in the polymer film. The polarized optical microscopy probe the film with conjugated rod-like PPQ block, thus, the bright

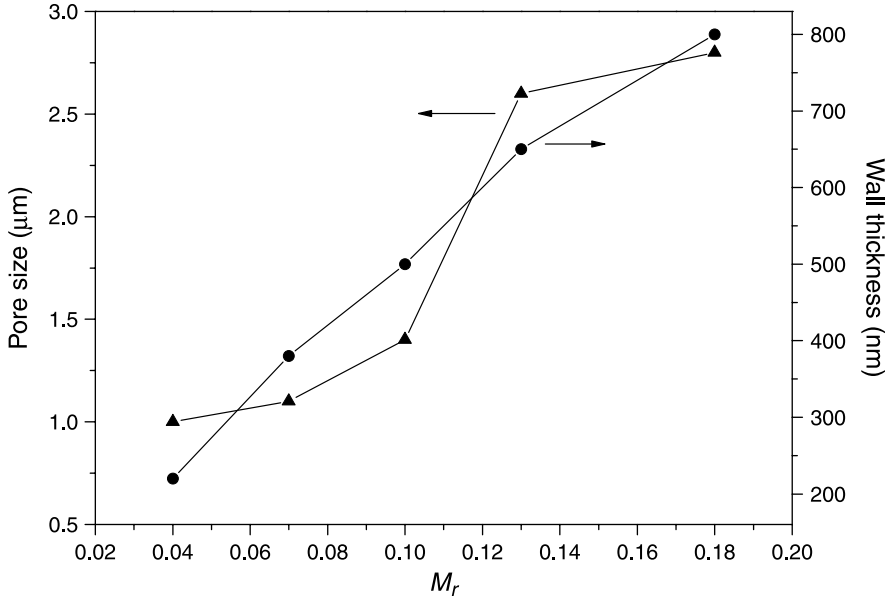

Fig. 9. The plot of pore size and wall thickness versus relative molecular mass (M_r) at constant polymer concentration of 1 wt%. Only five ratios are plotted, because the solubility of $PPQ_{120}PMMA_{800}$ is too poor to form the regular porous film.

structure in the figure corresponds to the rod-coil block copolymer.

Fig. 7 shows SEM images of the as-prepared honeycomb structures of PPQ-PMMA films from different concentrations of PPQ-*b*-PMMA solutions at a relative humidity of 75% and air flow rate of 2 m s^{-1} at room temperature. As can be seen in Fig. 7(a)–(c), larger pore sizes are obtained when using lower concentrations of the polymer solution: As the concentration of the polymer solution increased from 0.1 to 1 wt%, the pore size decreased from 2.3 to 1.2 μm.

We proposed that the relative molecular mass (M_r, PPQ block relative to PMMA block) is also an important factor in dictating the pore size, higher M_r resulting in higher pore size. At the same polymer concentration of these polymer solutions (1 wt%), the pore size of $PPQ_{48}PMMA_{1300}$ (ca. 1.1 μm) is about the same as that of $PPQ_{52}PMMA_{2500}$ (ca. 1 μm), as shown in Fig. 8(a) and (b), in which both diblock copolymers have different M_r values (0.07 vs. 0.04, Table 2). Nevertheless, the $PPQ_{52}PMMA_{800}$ (Fig. 8(c)) possessing a higher value of M_r (0.13) has a significantly larger pore size at 2.6 μm. The correlation of pore size and relative molecular mass is plotted in Fig. 9, where the higher M_r value is tend to form the larger pore size. From Fig. 8, the wall thickness between the pores is also strongly dependent on the value of M_r. As can be seen, the average wall thickness of the film formed by $PPQ_{52}PMMA_{2500}$ (M_r= 0.04) is ca. 220 nm. The wall thicknesses of the structures formed by $PPQ_{48}PMMA_{1300}$ (M_r=0.07) and PPQ_{50}-$PMMA_{800}$ (M_r=0.13) are ca. 380 and 650 nm, respectively. Other PPQ-PMMA copolymers possessing different values of M_r have the same tendency. The wall thickness for the PPQ-PMMA copolymer increases linearly with the increase of it relative molecular mass M_r, as shown in Fig. 9. Review Fig. 7 again, although the film was formed by different concentrations of $PPQ_{52}PMMA_{2500}$, the wall thicknesses of these films are the same (220 nm). Hence, the value of wall thickness can not be altered by other factors; it only depends on the value of M_r.

The mechanism of the 'breath figure' method has been proposed previously [30,34,38–40]. The high vapor pressure of the organic solvent drives solvent evaporation and rapidly cools the surface. This cooling leads to nucleation, and tiny water droplets cover the entire surface. Due to the incompatibility of the organic solvent and water, the polymer precipitates under this hydrophilic/hydrophobic balance and the polymer layer is formed [41,42]. Only this 'fast nucleation and slow growth' mechanism [43] provides the uniform size of the water droplets. These droplets are transported to the three-phase line and are hexagonally packed by the convectional flow or the capillary force generated at the solution front. After the solvent is evaporated, the membrane temperature rises up the ambient temperature and water contained inside the droplets evaporates by bursting the polymer film, leading to the formation of the circular holes network observed on the cross section of the membrane (Fig. 8(a)).

According the mechanism mentioned above, controlling the pore size by varying the concentration of polymer solution should have its limit. The polymer possesses a 'precipitate-like' behavior at the interface between the solution and water, and thus, creates a solid polymer envelope around the isolated water droplet. This polymer layer is able to prevent the coalescence of the water droplets to form the highly regular honeycomb structure [42]. Hence, at a very low concentration, the polymer is unable to support the stable polymer envelope and the water droplets tend to

coalesce with impulsive force to enlarge the pore size distribution and form the polygon structure as shown in Fig. 7(d).

4. Conclusions

Rod-coil diblock copolymers have been synthesized using the versatile ATRP method. This method is based on polymerizing MMA in the presence of a bifunctional initiator to obtain a methyl ketone-terminated PMMA. This functionalized PMMA was then copolymerized with 5-acetyl-2-aminobenzophenone to form the PPQ-*b*-PMMA diblock copolymer. The methyl ketone-terminated PMMA has a higher value of T_g than does the virgin PMMA because of its syndiotactic-like structure. The decomposition temperature (T_d) of the rod-coil diblock copolymer is higher than that of the PMMA homopolymer because the presence of the PPQ block retards the early decomposition of PMMA chains. Regular, porous honeycomb-structured films were prepared from the dichloromethane solution of the diblock copolymer in an air-flow hood. A higher polymer concentration results in larger pores, because the aggregation of polymer is fast. If the concentration of the polymer solution is too low, water droplet coalescence tends to enlarge the pore size and size distribution, and forms polygon structures. Higher relative molecular masse (M_r) tends to create larger pores. The wall thickness between the pores increases linearly with the increase of the relative molecular mass (M_r).

References

[1] Bates FS, Fredrickson GH. Annu Rev Phys Chem 1990;41:525.
[2] Matsen MW, Schick M. Curr Opin Colloid Interface Sci 1996;1:329.
[3] Radzilowski LH, Wu JH, Stupp SI. Macromolecules 1993;26:879.
[4] Li W, Maddux T, Yu L. Macromolecules 1996;29:7329.
[5] Jenekhe SA, Chen XL. Science 1998;279:1903.
[6] Chen XL, Jenekhe SA. Macromolecules 2000;33:4610.
[7] Jenekhe SA, Chen XL. J Phys Chem B 2000;104:6332.
[8] Agrawal AK, Jenekhe SA. Macromolecules 1993;26:895.
[9] Zhang X, Shetty AS, Jenekhe SA. Macromolecules 1999;32:7422.
[10] Agrawal AK, Jenekhe SA. Chem Mater 1993;5:633.
[11] Lapos JA, Wwing AG. Anal Chem 2000;72:4598. Clark RA, Hietpas PB, Ewing AG. Anal Chem 1997;69:259.
[12] Pris AD, Porter MD. Nano Lett 2002;2:1087.
[13] Cooper JM. Trends Biotechnol 1999;17:226.
[14] Troyer KP, Wightman RM. Anal Chem 2002;74:5370.
[15] Imhof A, Pine DJ. Nature 1997;389:948.
[16] Stenzel-Rosenbaum MH, Davis TP, Fane AG, Chen V. Angew Chem Int Ed 2001;40:3428.
[17] Maruyama N, Koito T, Nishida J, Sawadaishi T, Cieren X, Ijiro K, et al. Thin Solid Films 1998;327–329:854.
[18] Jenekhe SA, Chen XL. Science 1999;283:372.
[19] Erdogan B, Song L, Wilson JN, Park JO, Srinivasarao M, Bunz UHF. J Am Chem Soc 2004;126:3678.
[20] Yu C, Zhai J, Gao X, Wan M, Jiang L, Li T, et al. J Phys Chem B 2004;108:4586.
[21] Matyjaszewski K, Xia J. Chem Rev 2001;101:2921.
[22] Keller RN, Wycoff HD. Inorg Synth 1946;2:1.
[23] Sybert PD, Beever WH, Stille JK. Macromolecules 1981;14:493.
[24] Grohens Y, Prud'homme RE, Schultz J. Macromolecules 1998;31:2545.
[25] Bovey FA. Chain structure and conformation of macromolecules. NY, USA: Academic Press; 1982.
[26] Holland BT, Blanford CF, Stein A. Science 1998;281:538.
[27] Kulinowski KM, Jiang P, Vaswani H, Colvin VL. Adv Mater 2000;12:833.
[28] Velev OD, Jede TA, Lobo RF, Lenhoff AM. Nature 1997;389:447.
[29] Baker JT. Philos Mag 1922;56:752.
[30] Beysens D, Konbler CM. Phys Rev Lett 1986;57:1433.
[31] Family F, Meakin P. Phys Rev Lett 1988;61:428.
[32] Widawski G, Rawiso M, François B. Nature 1994;369:387.
[33] François B, Pitois O, François J. Adv Mater 1995;7:1041.
[34] Srinivasarao M, Collings D, Philips A, Patel S. Science 2001;292:79.
[35] Boer BD, Stalmach U, Nijland H, Hadziioannou G. Adv Mater 2000;12:1581.
[36] Karthaus O, Maruyama N, Cieren X, Shimomura M, Hasegawa H, Hashimoto T. Langmuir 2000;16:6071.
[37] Song L, Bly RK, Wilson JN, Bakbak S, Park JO, Srinivasarao M, et al. Adv Mater 2004;16:115.
[38] Stenzel MH, Davis TP, Fane AG. J Mater Chem 2003;13:2090.
[39] Stenzel MH. Aust J Chem 2002;55:239.
[40] Briscoe BJ, Galvin KP. J Phys D 1990;23:422.
[41] Pitois O, François J. Colloid Polym Sci 1999;277:574.
[42] Pitois O, François J. Eur Phys J B 1999;8:225.
[43] Maruyama N, Karthaus O, Ijiro K, Shimomura M, Koito T, Nishimura S, et al. Supramol Sci 1998;5:331.